A droplet platform capable of handling dissimilar liquids and its application for separation of bacteria from blood

Wu, Jiawei; Xia, Huanming; Wang, Wei; Foo, Yuhao; Wang, Zhiping; Du, Hejun

2020

Wu, J., Xia, H., Wang, W., Foo, Y., Wang, Z. & Du, H. (2020). A droplet platform capable of handling dissimilar liquids and its application for separation of bacteria from blood. Biomicrofluidics, 14(3). https://dx.doi.org/10.1063/5.0006111

https://hdl.handle.net/10356/148761

https://doi.org/10.1063/5.0006111

Biomicrofluidics ARTICLE scitation.org/journal/bmf

A droplet platform capable of handling dissimilar liquids and its application for separation of bacteria from blood

Cite as: Biomicrofluidics 14, 034102 (2020); doi: 10.1063/5.0006111
Submitted: 28 February 2020 · Accepted: 22 April 2020 ·
Published Online: 7 May 2020

Jiawei Wu,[1] Huanming Xia,[1,a)] Wei Wang,[2,a)] Yuhao Foo,[2] Zhiping Wang,[2] and Hejun Du[3]

AFFILIATIONS

[1]School of Mechanical Engineering, Nanjing University of Science and Technology, Nanjing 210094, People's Republic of China
[2]Singapore Institute of Manufacturing Technology, 73 Nanyang drive, Singapore 637662
[3]School of Mechanical and Aerospace Engineering, Nanyang Technological University, 50 Nanyang Avenue, Singapore 639798

[a)]**Authors to whom correspondence should be addressed:** hmxia@njust.edu.cn and wwang@simtech.a-star.edu.sg

ABSTRACT

For passive droplet generation, multiple parameters such as the fluid viscosities and flow rates of the continuous and discrete phases correlate to each other, raising relevant control difficulties. In the current study, a droplet platform that is capable of handling dissimilar liquids is proposed. Through combining oscillatory flow and electric charge, synchronized generation and forced coalescence of different droplets can be achieved. Its application for the separation of *E. coli* from blood is tested, which leads to a high capture efficiency with less sample and within a shorter time than usual.

I. INTRODUCTION

In the past few years, droplet microfluidics[1,2] has been proven as an effective tool for various chemical syntheses, biochemical analysis, and clinical diagnostics.[3–6] It provides some unique advantages such as ultra-high throughput, high accuracy, less sample, and reagent consumption. In its applications, an important topic involved is droplet manipulation, including droplet generation, transporting, sorting, splitting, and coalescence.[7–13] For passive droplet generation, the droplet volume and generation frequency are sensitive to the channel size, the flow rates, and properties of the continuous and discrete phases.[8] It raises the difficulty of relevant controls, especially in the cases where droplets of different sizes and viscosities must be simultaneously handled. To solve the problem, it relies on active droplet manipulation. For example, external mechanical vibrators can be applied to govern the droplet generation,[14–16] and electric fields[17,18] and surface acoustic waves (SAWs)[19] can facilitate droplet coalescence. Link *et al.*[18] proved that the presence of the electric field can make the droplet formation become exactly synchronized and make droplets coalesce more easily. However, the droplet size changes as the electric field changes and the droplet generation frequency varies with the droplet size. Bhattacharjee and Vanapalli[20] used the electrocoalescence method to do serial dilution. It allows on-demand and controlled dilution of droplets and is simple enough to be useful for assays that require serial dilutions.

In our previous work, we developed a negative-differential-resistance (NDR) microfluidic oscillator[21–23] and demonstrated its application for active droplet control.[24] Applied to the continuous phase, the device produces an oscillatory flow that governs the droplet formation. The droplet size can be independently controlled through tuning the flow rate of the discrete phase. Using one single oscillator, droplets of different volumes and viscosities can be generated synchronously, facilitating their subsequent one-to-one coalescence. However, it was also noted that under some conditions, e.g., the channels are not strictly symmetrical, it is rather difficult for the droplets to merge, especially when surfactant stabilizers are added. So, in the current work, an electric field is added to promote droplet coalescence. By converting the electric signal, the two discrete phases can be positively or negatively charged, respectively. Then, under the electric force, the generated droplets of the two distinct fluids can attract each other and merge more easily. Thus, utilizing the NDR microfluidic oscillator and in combination with the electric charge, a universal

droplet platform is developed, which favors various biological and chemical applications.

II. CHIP DESIGN AND EXPERIMENTAL SETUP

Figure 1(a) is a 3D schematic diagram of the droplet system. Upon flowing through the oscillator, the stable flow of the continuous phase turns into an oscillatory flow. Then, it splits into two streams and is applied to the T-junction droplet generators downstream. In such a design, within a wide range of the flow rate Q and viscosity μ of the discrete phase, the droplet generation frequency f keeps the same with that of the oscillator. An electric field is applied to the two discrete phases, so the generated droplets will be positively or negatively charged. Due to the electric attraction force, they approach each other and finally contact and coalesce in the downstream channel. Through changing the applied voltage, the magnitude of the attraction force can be adjusted. Figure 1(b) is a dimensional drawing of the droplet coalescence chip. The channel width at the T-junction is 250 μm, and for the rest part it is 500 μm. All the channels are 500 μm deep.

For the ease of observation, a transparent PMMA material was chosen to fabricate the chip. Conventional micro-milling and thermal bonding methods were used. The oscillator was designed in a plug-and-play manner as previously reported,[25] which is also shown in Fig. 1(c). In this way, the oscillator works as an independent unit, it also helps us to simplify the structure of the droplet chip. To generate water-in-oil (W/O) droplets, a hydrophobic coating (1700 Engineering Fluid, 3M, USA) was applied to modify the surface property of the channel. Two electrodes are embedded in the tubing transporting the discrete phases separately, and a DC power from a voltage converter (F30, XP POWER, Singapore) is used for the electric charge. 3M 7500 engineering fluid (3M, USA) is used as the continuous phase. It is delivered using a pressure pump. Its flow rate and the oscillation frequency are determined by the operating pressure. DI water–glycerol mixtures with/without dye are used as the discrete phase. They are infused into the droplet chip using two syringe pumps (Pump 11 Elite, Harvard apparatus, USA). A high speed video camera (FASTCAM SA5, Photron USA Inc.) is used to record the droplet generation and coalescence process. Based on the frame rate, the droplets generation frequency and their moving velocity can be calculated.

III. RESULTS AND DISCUSSION

A. Droplets generation and coalescence

Figure 2 compares the results with and without electric charge. Pure DI water is used as the discrete phase. For the first case shown in Fig. 2(a), the operating pressure of the oscillator, $P_o = 0.43$ bar and the oscillation frequency or the droplet generation frequency, $f \approx 102$ Hz. The flow rate of both the discrete phases is 50 μl/min, and the droplet volume is 8.2 nl. From Fig. 2(a.i), the droplets cannot coalesce together without electric charge. The droplets from both sides are generated synchronously. They reach the entrance of the downstream channel at about the same time and contact each other at 3.2 ms. Deformation of the droplets is observed as they experience squeezing to some extent. However, after that they soon move away from each other. At 3.9 ms, the distance between two droplets increases. At 7.1 ms, the two droplets recover into a normal spherical shape and form a stable droplet pair. In comparison, after applying a voltage of 800 V (V_d) to the discrete phases, the droplets attract each other and quickly collide and merge together at 2.7 ms [see Fig. 2(a.ii)].

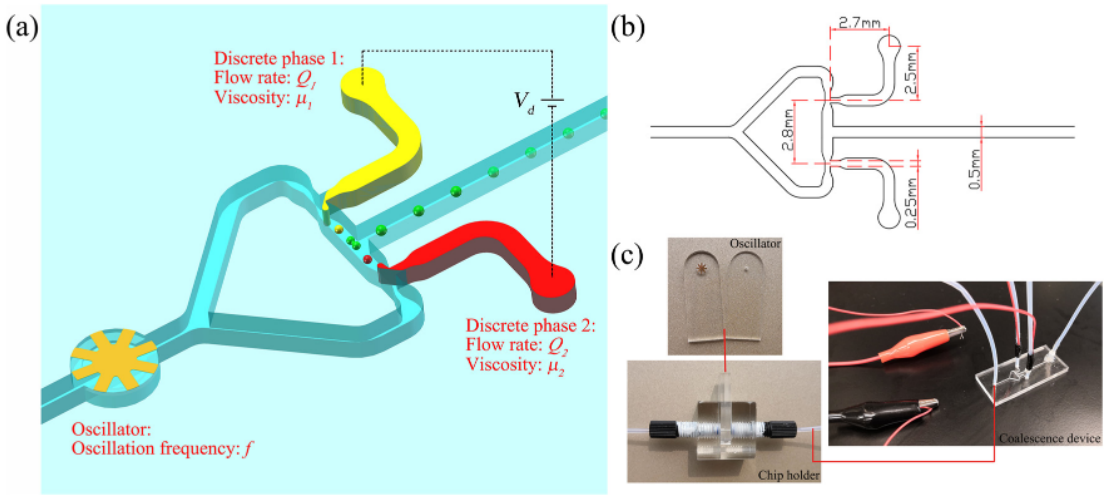

FIG. 1. (a) A 3D schematic diagram of the droplet system. The flow rates and viscosities of the two discrete phases are Q_1, Q_2 and μ_1, μ_2, respectively. The droplet generation frequency is f, which is the same as the oscillator oscillation frequency. (b) A dimensional drawing of the droplet coalescence chip. The channel width at the droplet generator (T-junction) is 250 μm. (c) The photograph of the oscillator designed as a plug-and-play module, and the droplet coalescence chip connected with electric cables.

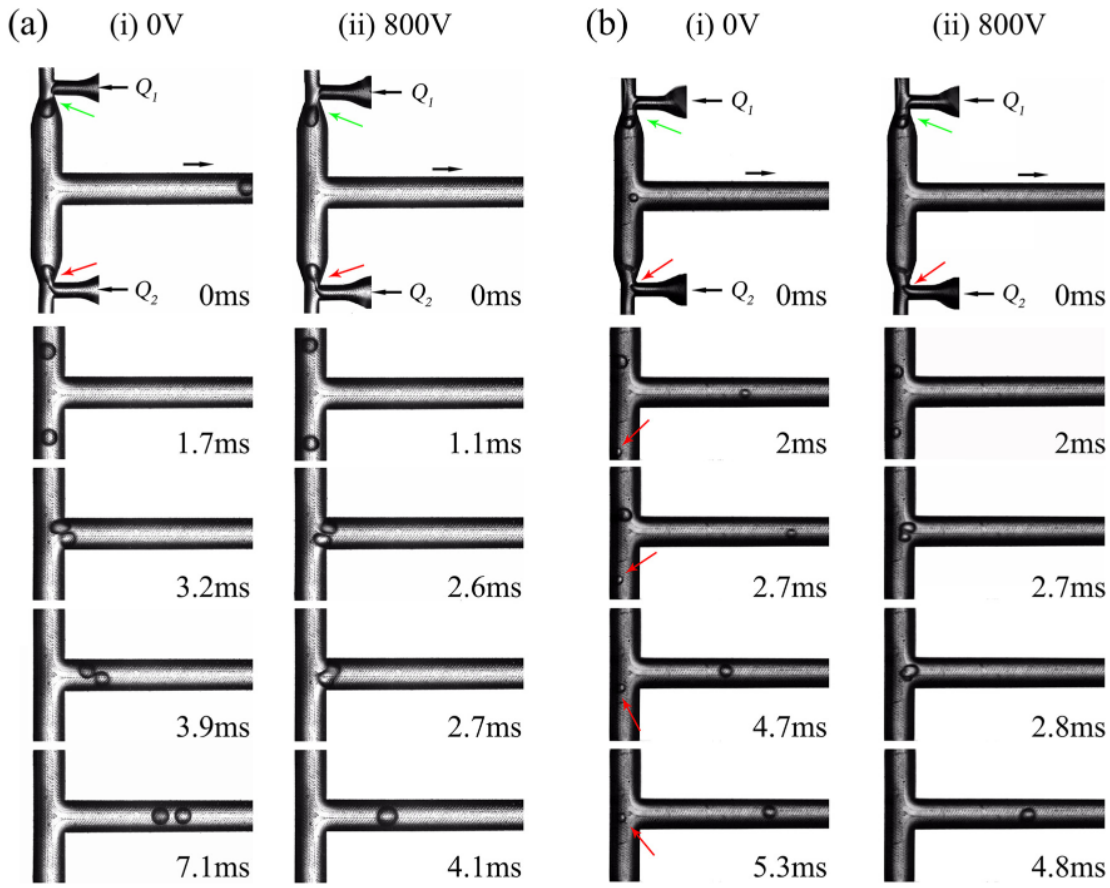

FIG. 2. Droplet coalescence with and without electric charge. (a) $Q_1 = Q_2 = 50\,\mu$l/min, $P_o = 0.43$ bar, (i) $V_d = 0$ V. (ii) $V_d = 800$ V (b)$Q_1 = 60\,\mu$l/min, $Q_2 = 30\,\mu$l/min, $P_o = 0.33$ bar, (i) $V_d = 0$ V, (ii) $V_d = 800$ V.

For the second case shown in Fig. 2(b), $P_o = 0.33$ bar, $f \approx 90$ Hz. The flow rates of the discrete phases are $60\,\mu$l/min and $30\,\mu$l/min, and the corresponding droplet volumes are 11.1 nl and 5.5 nl, respectively. It can be seen from the figure that the bigger droplet moves faster than the small one. This is because the flow rate of the first discrete phase is higher than that of the second one, $Q_{d1} > Q_{d2}$. Though the two droplets form synchronously under the oscillation, the bigger droplet enters the downstream channel a little bit earlier. Due to this mismatch between their velocities, the two droplets can hardly meet and coalesce. Figure 2(b.ii) illustrates the results after applying the electric charge at $V_d = 800$ V. At 2 ms, the big droplet is quite close to the downstream channel, while the small one is still a little far away. Though there still exists a slight mismatch between their velocities, the two droplets can quickly approach each other and eventually merge at 2.8 ms.

It is also found that under the electric force, the droplets move faster than that without electric charge. In Fig. 2(a), it takes 2.6 ms for the two charged droplets to get contact, which is 0.6 ms shorter than that without charging. In Fig. 2(b.ii), at 2.7 ms, both the droplets have a larger displacement than that in Fig. 2(b.i). To further analyze the influence of the electric charge, the moving behavior of the droplets in the channel is examined. With the two droplets approaching each other, the electric force will gradually increase and the droplets will be accelerated. Here, the time is recorded (Δt) starting from when the droplets reach a distance of $500\,\mu$m until they contact each other and start to coalescence. The results at different voltages are compared in Fig. 3. In all the tested cases, the operation pressure is 0.33 bar, the flow rate of both the discrete phases is $40\,\mu$l/min, and the corresponding droplet volume is 7.49 nl. At $V_d = 200$ V, it requires a longer time for the droplets to collide and coalesce, Δt is around 1 ms. As V_d increases to 800 V and 1200 V, Δt is reduced to 0.33 ms and 0.26 ms, respectively. This is believed due to the fact that raising the voltage will increase the electric force, as a result the acceleration of the droplets will become more and more significant. In addition, a large electric force is also beneficial to overcome the droplet surface intension (F_γ), which keeps the droplets in a spherical shape and hinders their coalescence. The average velocities of the droplets during this process are also calculated. The results are displayed in

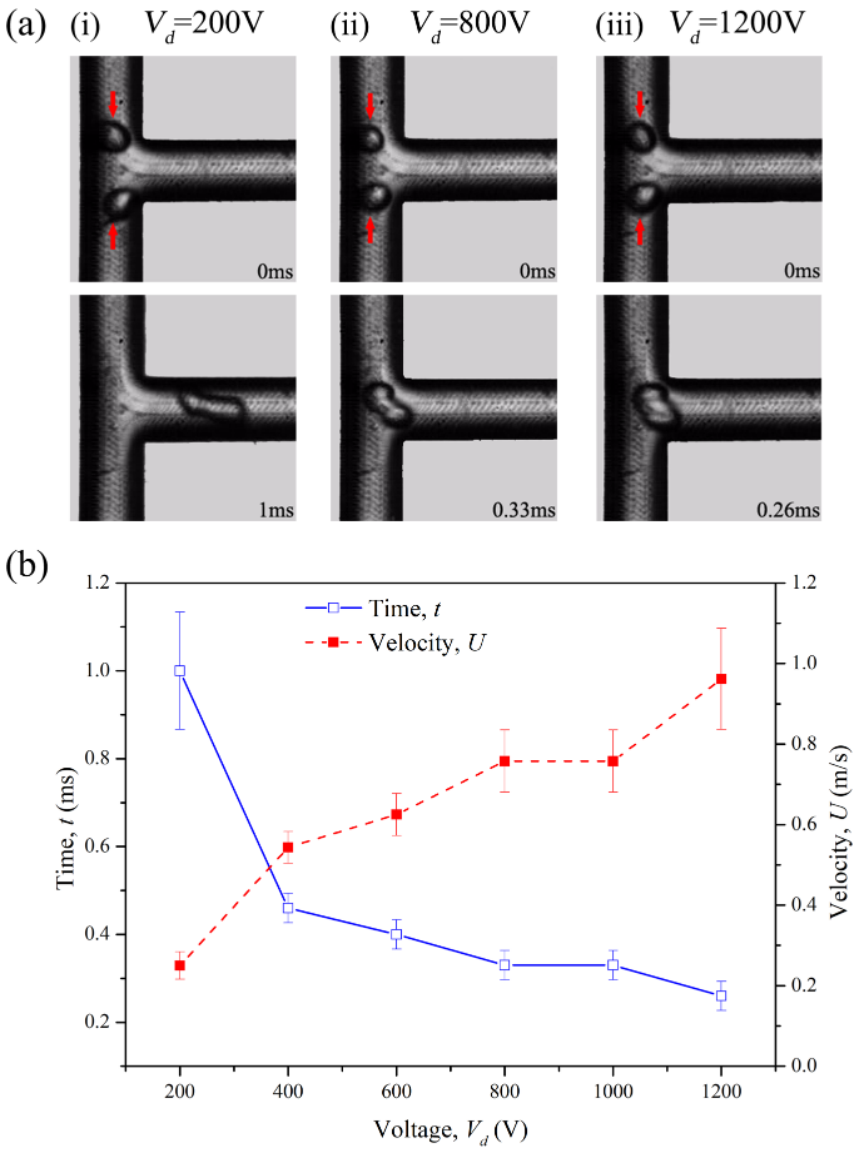

FIG. 3. (a) Approaching and coalescence of the droplets under voltage of (i) 200 V (ii) 800 V (iii) 1200 V. (b) Results of the averaged droplet velocity as they approach each other from a distance of 500 μm, and the time required for them to get contact and start to coalescence.

Fig. 3(b). Apparently, with the increase of the applied voltage, the droplet velocity rises up correspondingly and Δt is reduced. When V_d is increased from 200 V to 400 V, Δt drops sharply from 1 ms to 0.47 ms. The droplet velocity U_d increases from 0.25 m/s to 0.53 m/s. As has been mentioned, a higher voltage can boost the surface rupture of the droplets and ease the coalescence process. However, if the applied voltage is less than 200 V, the droplet cannot merge into one because of the weak attractive force. If the droplets are excessively charged (>1200 V), the electric force will become so large that it may seriously distort the droplet and even break it into several smaller ones.

The success rate of droplet coalescence (χ) under different conditions is also examined. For the above-mentioned case at droplet size of 7.49 nl, χ is 71.4% at $V_d = 200$ V. At $V_d = 400$ V and above, all the droplets can coalesce, i.e., χ is 100%. It is noticed that besides the electric voltage V_d, χ is also influenced by the droplet size. In another test, the droplet size is increased to 22.5 nl. The coalescence success rate is $\chi = 0\%$, 86.7%, 100% at $V_d = 100$ V, 200 V, and 300 V, respectively.

Theoretically, the droplets inside the continuous flow are subjected to multiple forces.[26] The competition among the shearing force, viscous force, and interfacial tension determines the droplet formation process, while the coalescence behavior of water droplets in oil can be described in three stages: droplets approaching each other, the process of film thinning/drainage, and film rupture leading to droplet–droplet coalescence.[27] Coalescence of the water

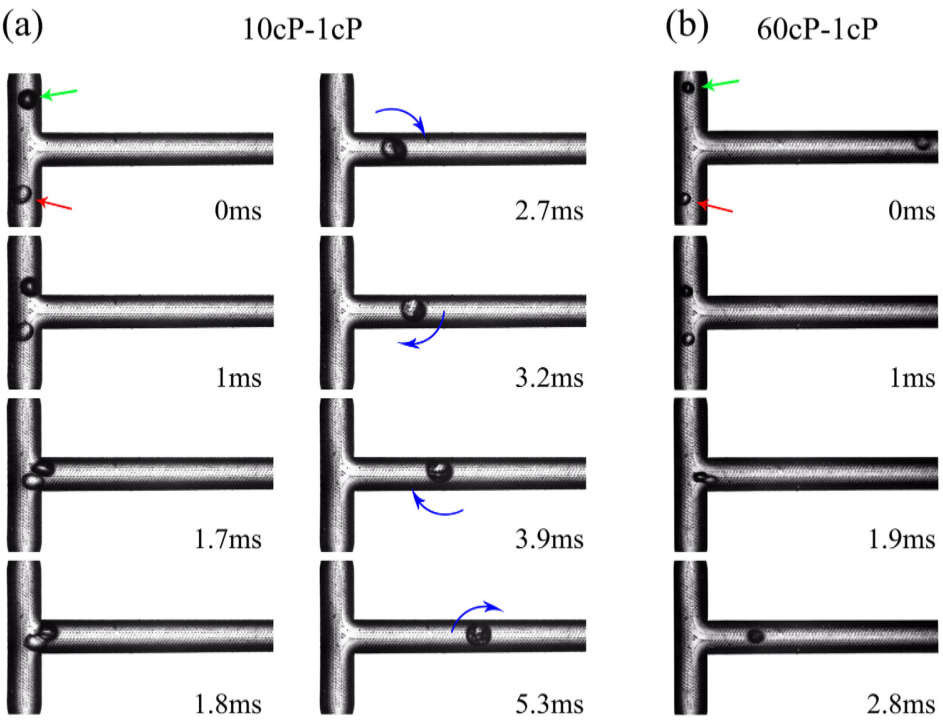

FIG. 4. The droplet coalescence process at viscosity ratio of (a)10, and (b) 60.

droplets in oil is induced by dynamically destabilizing the interfacial oil film between the droplets, which are brought together to a very close distance by a competition flow in the constricted microchannel. When the droplets are positively and negatively charged, respectively, the attractive force (Coulomb force) between them accelerates the droplet motion, approaching and thus thinning of the oil film between droplets to lead to instability of the film. On the other hand, the applied electric field polarizes the droplets, promotes contact between droplets, and exerts electrohydrodynamic forces across the interfacial film. Thus, as shown in Fig. 2(a), droplets start being coalesced to each other when the droplet charging is turned on.

Droplets with different viscosity ratios are also tested. One discrete fluid is DI water. The other one is DI water–glycerol mixture. Through changing their volume ratio, the mixtures of 10cP and 60cP are prepared. The applied voltage is fixed at 800 V and the operation pressure is 0.3 bar. Relevant results are demonstrated in Fig. 4. For the first case, the flow rate of both the discrete phases is 50 μl/min, the droplet size is 8.8 nl, and the viscosity ratio is 10. From Fig. 4(a), the two droplets are generated synchronously. Then, under the electric force, they approach each other and coalesce together at 1.8 ms. After that, the merged droplet gradually recovers the spherical shape at 2.7 ms. As the merged droplet volume is just 17.6 nl, at such a small scale, the mixing of the two fluids within the droplet is rather difficult. In the subfigure of 2.7 ms, the fluid interface can be clearly observed. It is also found that, most probably due to some asymmetrical factors such as the velocity mismatch between the two droplets, after merging it has caused rapid rotation of the droplet. The rotation will enhance the mixing process. As can be seen, after just 2.6 ms (t = 5.3 ms), the fluid interface has become rather blur due to mixing. For the second case [see Fig. 4(b)], the flow rate of both the discrete phases

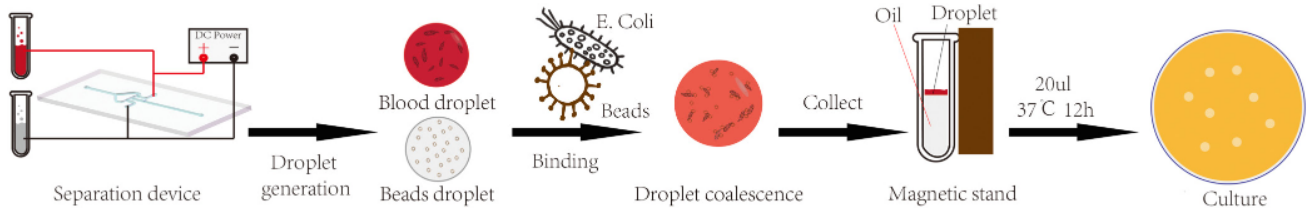

FIG. 5. Schematic showing the procedures for separation of *E. coli* from blood.

TABLE I. Capture efficiency of *E. coli* from blood.

Method	Testing cases	*E. coli* concentration, C_E (CFU/ml)	Flow rate, Q (μl/min)	Beads concentration, C_b	Capture efficiency, η
Current method	1	0.89×10^5	100	4×10^6 beads/ml	98.03%
	2			4×10^7	99.33%
	3			4×10^8	No *E. coli* observed in the supernatant.
Segmented-flow method[29]	1	5×10^5	80	5×10^{10}	~91.5%
	2		120		~90.5%
Biospleen device in vitro[30]	1	10^4	~174	0.5 mg/ml	~90%

is 30 μl/min, the corresponding droplet volume is 3.4 nl, the viscosity ratio is increased to 60. Results show that despite the large difference in their viscosities, the two droplets can still be generated synchronously. Reliable droplet coalescence is also achieved.

B. Application for separation of *E. coli* from blood

Application of current droplet platform for bacteria separation from blood was tested using *Escherichia coli* (*E. coli*) as an example. Reliable detection of *E. coli* from blood samples is of significance for early diagnosis of sepsis.[28] The immunomagnetic bead separation method is used, and its operation procedures are displayed in Fig. 5. First, rabbit blood is diluted with PBS at 1:9. Then, *E. coli* and Apolipoprotein H (ApoH) magnetic beads (ApoH-Technologies, France) are separately added to the sample, and they are used as the discrete phases. If the passive droplet method is used, the slight difference in viscosities of the two discrete phases and the fabrication error in the droplet generators will cause a mismatch between the two droplet generation frequencies. Utilizing the current system, the blood droplets containing the bacteria and magnetic beads are synchronously formed and coalesced. Within the coalesced droplet, *E. coli* and the beads are well mixed to gain a high binding efficiency. After that, all the droplets are collected in a tube and the beads with bacteria are immobilized by the magnetic stand. Next, 20 μl supernatant of the blood solution is collected and is transferred onto the agar plate for further analysis. After culturing for 12 h in the incubator (37 °C), through counting the *E. coli* colony numbers on the agar plate, the bacteria capture efficiency can be calculated.

In the actual experiments, the operation pressure of the oscillator is kept at 0.3 bar. The flow rate of both the discrete phases is 50 μl/min. The applied voltage is 400 V. Some relevant results are presented in Table I. For the sample of *E. coli* concentration, $C_E = 0.89 \times 10^5$ CFU/ml, at a bead concentration of $C_b = 4 \times 10^6$ beads/ml, the capture efficiency η can reach 98.03%. At $C_b = 4 \times 10^7$ beads/ml, η increases to 99.33%. When C_b further increases to 4×10^8 beads/ml, no *E. coli* is observed in the supernatant, meaning that almost all the bacteria have been separated away from the blood. The current data are compared with some previously reported results. Suhanya *et al.*[29] studied *E. coli* separation from blood using a segmented-flow microfluidic device. The blood sample containing both the *E. coli* and the beads is segmented by air bubbles for mixing enhancement. As shown in Table I, at similar flow rates, the current method exhibits a higher capture efficiency at lower *E. coli* concentrations using less magnetic beads. In another study by Kang *et al.*,[30] a biospleen device was applied, which used an in-line spiral mixer and an incubation loop to promote the nanobead–pathogen binding. At an *E. coli* concentration of 10^4 CFU/ml, the capture efficiency η is up to about 90%. In comparison, a higher capture efficiency is achieved using the current method.

IV. CONCLUSIONS

In summary, a facile microdroplet platform is proposed. Despite the variety of applied fluids, by dint of a NDR oscillator, two different droplets can be synchronously generated. Their sizes are controllable individually through directly tuning the flow rate of the corresponding discrete phase. Then, a DC electric field is applied to charge the generated droplet pairs, which can greatly promote their one-to-one coalescence. Application of the system for separation of *E. coli* from blood was examined. The droplets carrying the blood sample and the magnetic beads can be fused reliably and, due to the enhanced mixing, a high capture efficiency can be obtained. In view of the fact that practical applications will involve various fluids of different properties, the current technique will help us to extend the applicable scope of droplet microfluidics.

ACKNOWLEDGMENTS

This work was supported, in part, by the National Natural Science Foundation of China (NNSFC, No. 51575282), the Fundamental Research Funds for the Central Universities (No. 30915118803), the CSC Scholarship (No. 201806840039), Nanyang Technological University, and the Singapore Institute of Manufacturing Technology under the Agency for Science, Technology and Research (A*STAR, Singapore).

DATA AVAILABILITY

The data that support the findings of this study are available from the corresponding author upon reasonable request.

REFERENCES

[1]S. Y. Teh, R. Lin, L. H. Hung *et al.*, Lab Chip **8**(2), 198–220 (2008).
[2]H. N. Joensson and S. H. Andersson, Angew. Chem. Int. Ed. **51**(49), 12176–12192 (2012).

[3]E. Y. Basova and F. Foret, Analyst **140**, 22–38 (2015).
[4]E. Hondroulis, A. Movila, P. Sabhachandani, S. Sarkar *et al.*, Biotechnol. Bioeng. **114**, 705–709 (2017).
[5]H. Yuan, Y. Pan, J. Tian, Y. Chao, J. Li, and H. Cheung Shum, Sens Actuators B Chem. **298**, 126766 (2019).
[6]Y. Liu and M. Walther-Antonio, Biomicrofluidics **11**(6), 061501 (2017).
[7]W. Wang, C. Yang, Y. Liu, and C. M. Li, Lab Chip **10**, 559–562 (2010).
[8]P. Zhu and L. Wang, Lab Chip **17**, 34–75 (2016).
[9]A. L. I. Lashkaripour, A. A. Mehrizi, M. Goharimanesh, M. Rasouli, and S. R. Bazaz, J. Mech. Med. Biol. **18**, 1850002 (2018).
[10]K. Kelemen, S. Gepperth, R. Koch, H. J. Bauer, and H. P. Schuchmann, Microfluid. Nanofluid. **19**, 1139–1158 (2015).
[11]A. Shams Khorrami and P. Rezai, Biomicrofluidics **12**(3), 034113 (2018).
[12]J. Park, J. H. Jung, K. Park, G. Destgeer, H. Ahmed, R. Ahmad, and H. J. Sung, Lab Chip **18**, 422–432 (2018).
[13]L. Mazutis and A. D. Griffiths, Lab Chip **12**, 1800–1806 (2012).
[14]A. Sauret, C. Spandagos, and H. C. Shum, Lab Chip **12**, 3380–3386 (2012).
[15]L. Schmid and T. Franke, Appl. Phys. Lett. **104**, 133501 (2014).
[16]V. Miralles, A. Huerre, H. Williams, B. Fournié, and M. C. Jullien, Lab Chip **15**, 2133–2139 (2015).
[17]A. R. Guzman, H. S. Kim, P. de Figueiredo, and A. Han, Biomed. Microdevices **17**, 35 (2015).
[18]D. R. Link, E. Grasland-Mongrain, A. Duri *et al.*, Angew. Chem. Int. Ed. Engl. **118**, 2618–2622 (2006).
[19]M. Sesen, A. Fakhfouri, and A. Neild, Anal. Chem. **91**, 7538–7545 (2019).
[20]B. Bhattacharjee and S. A. Vanapalli, Biomicrofluidics **8**(4), 044111 (2014).
[21]H. M. Xia, Z. P. Wang, W. Fan, A. Wijaya, W. Wang, and Z. F. Wang, Lab Chip **12**, 60–64 (2012).
[22]H. M. Xia, Z. P. Wang, V. B. Nguyen, S. H. Ng, W. Wang, F. Y. Leong, and D. V. Le, Appl. Phys. Lett. **104**, 024101 (2014).
[23]H. M. Xia, J. W. Wu, and Z. P. Wang, J. Micromech. Microeng. **27**, 075001 (2017).
[24]Y. Y. Zhang, H. M. Xia, J. W. Wu, J. Zhang, and Z. P. Wang, Appl. Phys. Lett. **114**, 073701 (2019).
[25]J. W. Wu, H. M. Xia, Y. Y. Zhang, S. F. Zhao, P. Zhu, and Z. P. Wang, Microsyst. Technol. **25**, 2741–2750 (2019).
[26]H. M. Sadeghi, B. Sadri, M. A. Kazemi, and M. Jafari, J. Colloid Interface Sci. **532**, 363–374 (2018).
[27]J. S. Eow, M. Ghadiri, A. O. Sharif, and T. J. Williams, Chem. Eng. J. **84**, 173–192 (2001).
[28]K. Reinhart, M. Bauer, N. C. Riedemann *et al.*, Clin. Microbiol. Rev. **25**(4), 609–634 (2012).
[29]D. Suhanya, R. G. Wu, Z. P. Wang, in *23rd International Conference on Miniaturized Systems for Chemistry and Life Sciences (μTAS 2019), Switzerland, October* (The Chemical and Biological Microsystems Society, 2019), pp. 730–731.
[30]J. H. Kang, M. Super, C. W. Yung *et al.*, Nat. Med. **20**(10), 1211 (2014).